ORIGINAL PAPER - PRODUCTION GEOLOGY

Impact of rock fabric on flow unit characteristics in selected reservoir sandstones from West Baram Delta Offshore, Sarawak

I. Yusuf[1,2] · E. Padmanabhan[1]

Abstract

The successful application of enhance oil recovery (EOR) technology requires an accurate understanding of the internal architecture of reservoirs and complex distribution of flow unit characteristics within different lithofacies. However, flow unit characteristics in the reservoir lithofacies of West Baram Delta Offshore, Sarawak, remain unexplored. Therefore, this paper investigates potential hydraulic flow units (HFUs) present within the five (5) identified sandstone lithofacies using thin sections, scanning electron microscopy (SEM), two-dimensional (2D) petrographic image analysis and helium porosimetery. The identified lithofacies include massive coarse-grained sandstone (MCGS), massive medium-grained sandstone (MMGS), massive fine-grained sandstone (MFGS), massive friable fine sandstone (MFFS) and massive very fine grained sandstone lithofacies (MVFGS). A plot of reservoir quality index (RQI) against normalized porosity (ϕz) showed five main hydraulic flow units (HFUs) within the identified lithofacies. The MFGS, MFFS and MVFGS lithofacies exhibited moderate to high matrix fractions and moderate to poor sorting, suggesting high tortuosity and hence characterized by low flow zone indicator (FZI). On the other hand, the MCGS and MMGS lithofacies exhibit very low to low matrix fractions, medium to coarse grain sizes and moderate to well sorting, signifying lower tortuosity, and hence characterized by relatively higher flow zone indicator (FZI). Thus, a hydraulic flow unit (HFU) can be formed by more than one lithofacies that exhibit similar fluid characteristic attributes, regardless of the difference in depositional environment and diagenetic processes undergone. This study concludes that HFU scattered plot can serve as a qualitative model for the characterization of flow unit characteristics in a well-comprising different lithofacies, particularly for field development plans in the West Baram Delta.

Keywords Rock fabric · Flow unit characteristic · Flow zone indicator (FZI) · Reservoir quality index (RQI) · West Baram Delta

Introduction

The successful application of enhanced oil recovery technology requires an accurate understanding of the multi-pore architecture attributes of different lithofacies that reflect varying depositional environments and petrophysical properties (Ebanks Jr 1987; Korvin 2016; Onuh et al. 2017; Terry et al. 2013). The Baram Field is the most prolific basin in West Baram Delta and has the most mature reservoir (Latief et al. 2012). It has been slated for enhanced oil recovery (EOR) to maximize oil production in the existing 170 wells (Abdullah 2012; Khatib 2012; Latief et al. 2012). However, flow unit characteristics in the different reservoir lithofacies of West Baram Delta Offshore, Sarawak, remain unexplored. Therefore, an accurate discrimination of potential hydraulic fluid units (HFU's) in the different lithofacies is vital for effective recovery ratio assessment and development of pathways plans in the area (Nooruddin and Hossain 2011; Prince et al. 1999; Zhou et al. 2014). This study first identifies the dominant lithofacies of the Baram Field, and then delineates the potential fluid flow units in the different lithofacies relative to their distinct porosity–permeability properties.

✉ I. Yusuf
  ishaq.yusuff@gmail.com

1 Department of Geosciences, Faculty of Geosciences and Petroleum Engineering, Universiti Teknologi PETRONAS, 32610 Seri Iskandar, Perak, Malaysia

2 Department of Geology and Mining, Faculty of Applied science and Technology, IBB University, Lapai, Niger State, Nigeria

The concepts of reservoir quality indicator (RQI) and fluid zone index

Archie (1952) was the first to describe and group similar geological (mineralogical, grain-pore compositions and diagenetic features) and petrophysical properties that control fluid flow (Hearn et al. 1984). Hydraulic flow units (HFU's) related to unique Flow Zone Indicator (FZI) have been developed from core analysis, reservoir quality index (RQI) (ratio between permeability and porosity) and normalized porosity (ratio between pore volume and grain volume) (Amaefule et al. 1993; Tiab and Donaldson 2015).

FZI has also been derived from rock texture and pore geometry attributes to pore volume, pore throat size, length, connectivity and tortuosity (Amaefule et al. 1993) with permeability estimated from uncored well using the Kozeny–Carman equation (Davies and Vessell 1996; Shenawi et al. 2007).

Porosity and permeability obtained using the Helium porosimetry system is used to define Flow Zone Indicator (FZI). The concept of reservoir quality index (RQI) is used to determine FZI (Amaefule et al. 1993). This approach entails the clustering of different sandstone lithofacies of similar internal textural grain–pore compositions and petrophysical properties (Ebanks Jr 1987). The RQI in μm of each core plug is calculated using the equation below (Amaefule et al. 1993):

$$RQI = 0.0314\sqrt{K}/\emptyset, \tag{1}$$

where RQI denotes Reservoir Quality index (μm), K permeability (mD), and Φ signifies fractional porosity.

To define the Flow Zone Indicator, RQI is plotted in log–log against normalized porosity (Φz). Φz is defined as the ratio of pore volume to grain volume ratio, while Flow Zone Indicator relates to RQI as $\Phi_z = 1$. Φz is determined as

$$\Phi z = \frac{V_p}{V_g} = \frac{\Phi}{1 - \Phi}, \tag{2}$$

where V_P denotes volume of pores, V_g volume of matrix, and Φ signifies porosity.

The flow zone indicator (FZI) is calculated using

$$Z = \frac{1}{Sgv \sqrt{Kz}}. \tag{3}$$

Similar FZI is indicated by plots of internal grain–pore geological composition and petrophysical properties lying on a straight line.

Regional geology and tectonic setting of the Sarawak Basin

The West Baram Delta is among the significant geological provinces located offshore Sarawak foreland Basin in Malaysia (Tan et al. 1999). The Baram Delta extends from the northern part of Sarawak to far southern Sabah (Fig. 1) with a total coverage area of 7500 km^2 by 2500 km^2 (Abdulrahman et al. 2014; Fui 1978; Rijks 1981). The province is extensively faulted by a major northeastern heading fault zone known as the West Baram Line that forms the western margin of the province (Tan et al. 1999). The closure and uplift of Late Cretaceous–Eocene proto-South China sea suggest the Sarawak Basin is a post-orogenic fore-land basin (Madon 1999). The erosion of the uplifted Rajang Fold–Thrust Belts hinterland during the Neogene and several tectonism facilitated sediment supply into the basin (Madon et al. 2013). The basin is underlain by more than 12,000 m of Tertiary siliciclastic and carbonate sediments (Doust 1981). The Sarawak margin was the site of southward subduction of a proto-South China sea oceanic crust (Cullen 2014) during Late Cretaceous to Pleistocene times and ended with the collusion of Luconia and West Borneo blocks.

Sedimentology and stratigraphy of the West Baram Delta

The offshore stratigraphic succession of the West Baram Delta is characterized by the occurrence of coastal to coastal-fluviomarine sand that has been deposited in a northwestwards prograding delta since the Middle Miocene (from Cycle IV onwards) (Tan et al. 1999). Periods of delta outbuilding are separated by rapid transgression, which is represented by marine shale interval at the base of the sedimentary cycles (Fui 1978). The regressive sands of each cycle grade northwestwards into neritic, mainly shaly sediments. An estimated thickness of about 6–9-km Neogene clastic sediment of coastal to coastal marine sands and shales make up the stratigraphy of the delta (Johnson et al. 1989). Fui (1978). Eight sedimentary cycles were identified in nearby onshore province of Sarawak Basin and were extended to the Baram Delta (Fig. 2). These cycles are either clastic or carbonate successions separated by noticeable shale intervals deposited during rapid transgression (Madon 1999). The major reservoir intervals in the Baram Delta that formed the Cycles V and VII began at the end of Middle Miocene where a sea level drop disrupted the carbonate deposition in Central Laconia and progressed until Early Pliocene era (Madon 1999). Within the Cycles V and VI, the preservation of well-developed
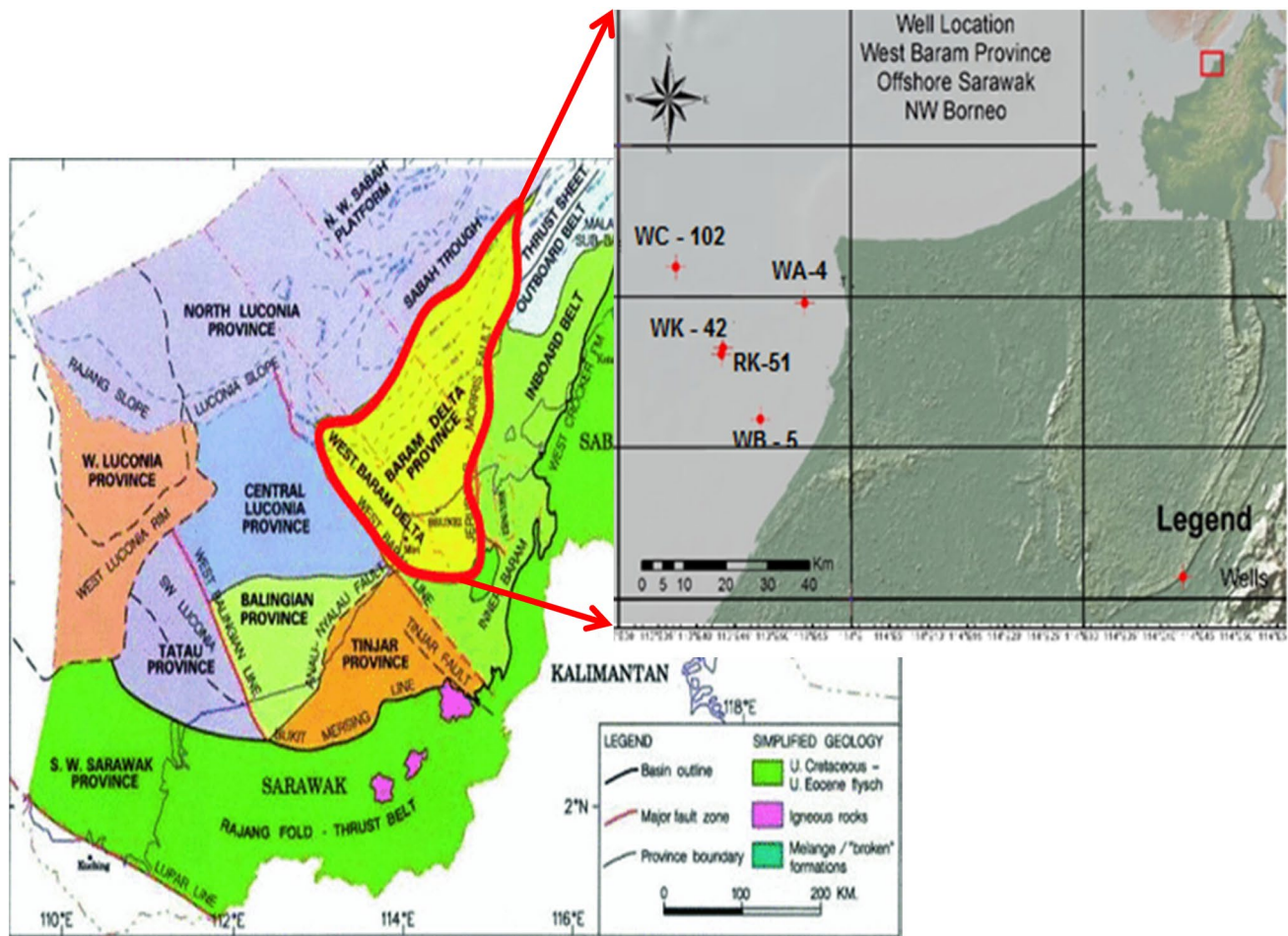
Fig. 1 Regional geology and well location map, modified after Madon (1999)

sequences is linked to high rapid sedimentation and subsidence within the delta. The distribution of the lithofacies indicates that waves and tidal currents are the two main important hydrodynamic processes controlling the present-day sedimentation in Baram Delta (Abdulrahman et al. 2014; Lambiase et al. 2002).

Materials and methods

A total of 97 subsurface cored samples and 1.5-inch core plugs were obtained from five exploratory wells in four fields drilled into the Cycles IV–V (early Miocene to upper Miocene) productive reservoir unit succession in offshore—Sarawak, Malaysia. The five wells comprise two appraisal wells (WA-4 from W-Field and WB-5 from Q-Field) and three deviated wells (WC-102 from R-Field, WK-42 and RK 51 from Z-Field) (see Fig. 1). The core samples were characterized into five distinct sandstone lithofacies based on their textural variations.

The rock fabrics of the samples were derived from petrographic studies using thin sections (Raith et al. 2011) and scanning electron microscopy (SEM) to visualize grain–pore distribution in each studied lithofacies. Textural characteristics were quantified from thin-section micrographs using 2D petrographic image analysis application that involved thresholding processing of grain–pore components. The quantified grain–pore textural characteristic includes grain sizes, shapes, orientation, pore sizes and grain sorting/packing (Boggs 2009). The 2D image-quantified values of the different grain shapes in each lithofacies were analyzed using sedimentological scale for variable grain sizes and roundness (Powers 1953; Wentworth 1922), respectively. The porosity and permeability data were obtained using the Helium porosimetery system. The equipment measures permeability within the range of 0.001 mD–10 D and porosity of up to 60% under maximum confining pressure of 400 Psi, at a room temperature between 25 and 27 °C and humidity range of 65–71%. The system calculated porosity using Boyle's and Charles' laws. The measurements were
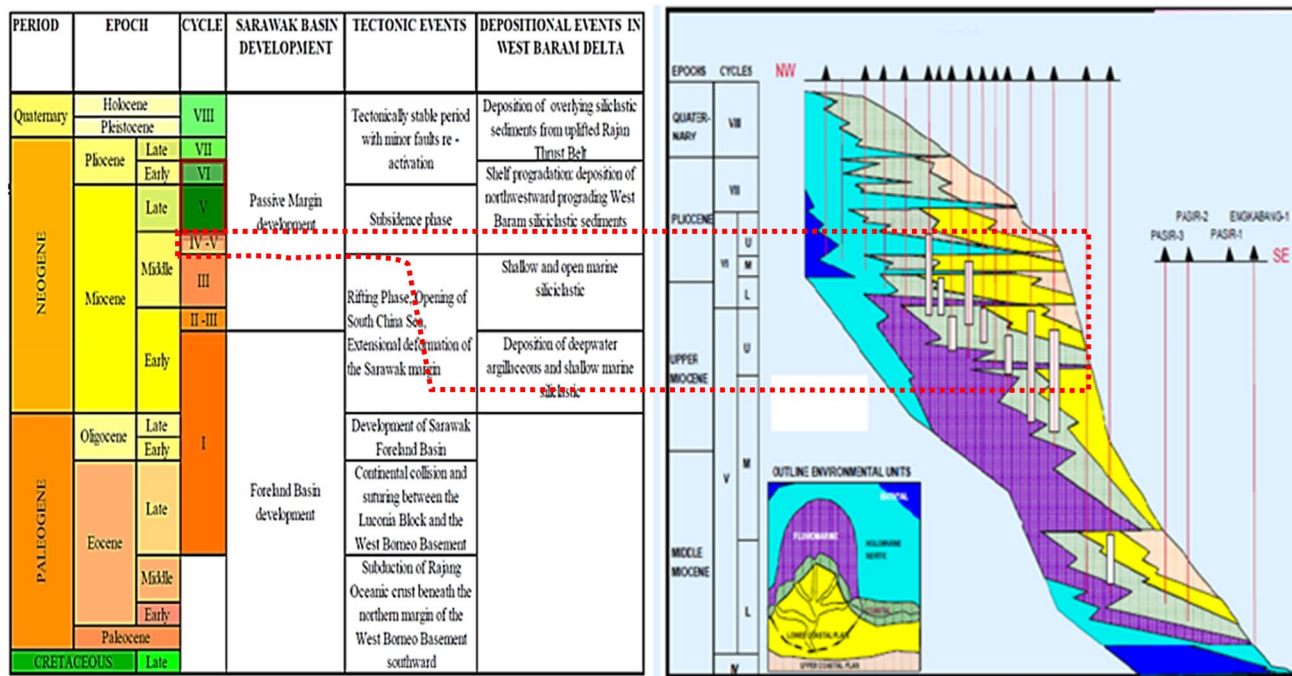
Fig. 2 Generalized stratigraphic column and framework for the Sarawak Basin, tectonics and depositional events in the West Baram delta, modified after Fui (1978), Madon (1999), and Pauzi et al. (1999)

performed according to the American Petroleum Institute recommendation practice 40 (API RP 40).

Results and discussion

The core description and characterization of the 97 subsurface samples reveal five main lithofacies, namely Lithofacies 1 consists of massive coarse-grained sandstones (MCGS), Lithofacies 2 comprises massive medium-grained sandstone (MMGS), Lithofacies 3 includes massive fine-grained sandstone (MFGS), Lithofacies 4 consists of massive friable fine-grained sandstone (MFFGS), and Lithofacies 5 consists of massive very fine grained sandstone (MVFGS) shown in Fig. 3.

Lithofacies 1: massive coarse-grained sandstone (MCGS)

15 samples were obtained for the MCGS lithofacies (Fig. 3a). The petrographic analysis of this lithofacies shows the presence of predominantly polycrystalline quartz grains that are oriented at > 120° (Fig. 4). The fine-grained matrix consists of siderite and iron oxides. The intergranular pore spaces are obliterated by quartz cement and growth (Fig. 5) as well as pore-filling kaolinite clay (Fig. 4), which indicates moderately high temperature and pressure of early phase diagenesis (Worden and Morad 2000). The relatively less

matrix content is attributed to deposition in higher energy level environment (Boggs 2009). This lithofacies reveals predominance of sub-rounded to well-rounded coarse grains complimented with moderate to well-sorted grains, which suggests far distance from source (Pettijohn et al. 1973). The thin-section images also showed the abundance of float and point contact grain packing. The intergranular and fracture porosities of this lithofacies vary from 24 to 34% and averaged at 25%. However, the resulting abundance of intergranular porosity within this lithofacies was reduced by burial and diagenesis. The presence of fracture porosity is possibly due to the prevalent tectonic processes that occurred in the delta after deposition (Tan et al. 1999).

The variation in porosity is mainly ascribed to grain–pore mineral composition and alterations exhibited in form of pore-filling (Fig. 4) and quartz growth/cementation (Fig. 5).

Lithofacies 2: massive medium-grained sandstone lithofacies (MMGS)

21 samples were selected from massive medium-grained sandstone lithofacies (MMGS) (Fig. 3b). Petrographic analysis (Fig. 6) of this lithofacies shows the dominant presence of medium quartz at variable grain sizes and shapes (Fig. 7). The quartz grains are predominantly monocrystalline and make up 38% of the total composition. The lithofacies is characterized by straight grain boundary, which is indicative of moderate or slight compaction of sediments
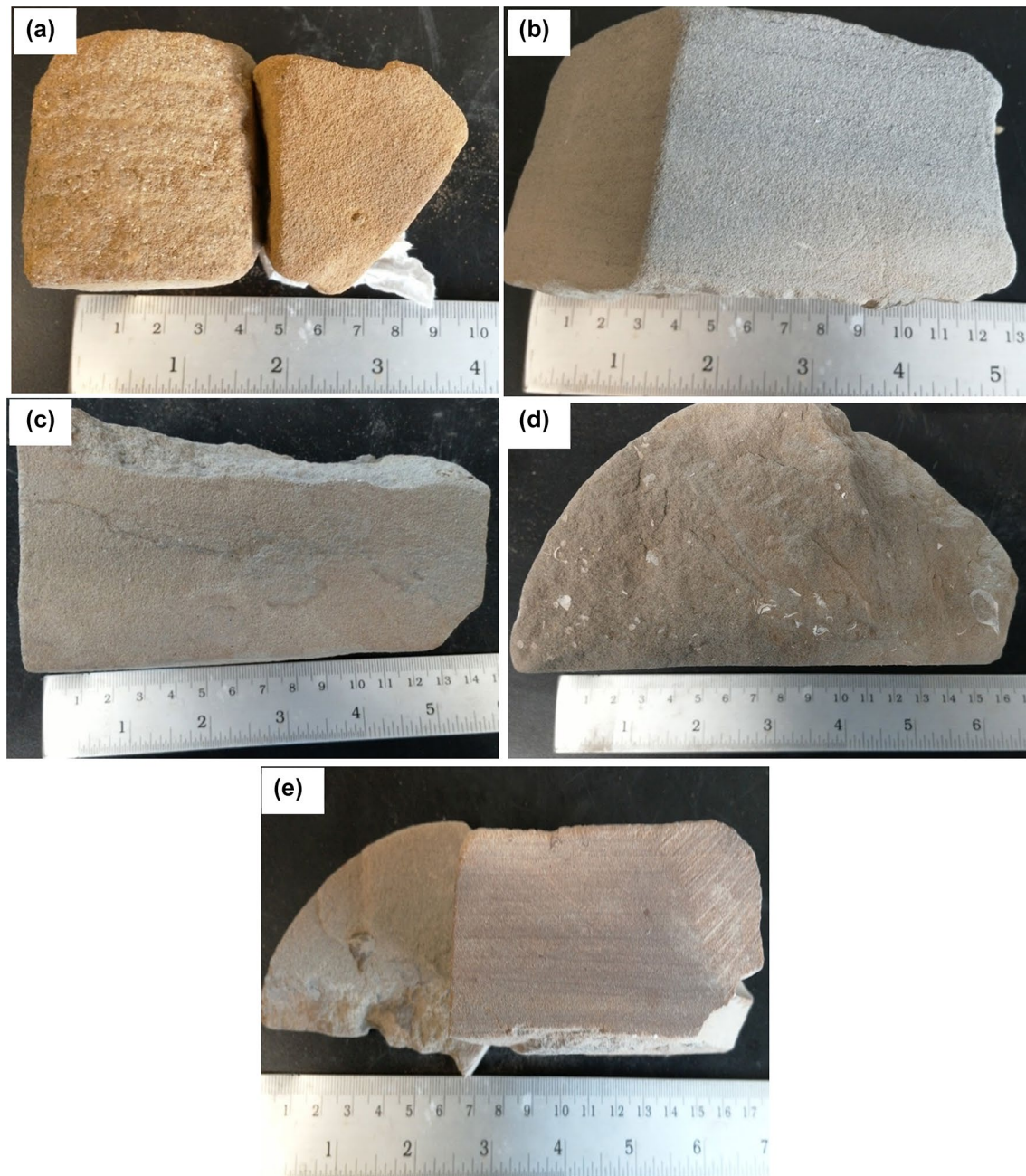
Fig. 3 Core specimen lithofacies. (**a**) Lithofacies 1: massive coarse-grained sandstone (MCGS), (**b**) Lithofacies 2: massive medium-grained sandstone (MMGS), (**c**) Lithofacies 3: massive fine-grained sandstone (MFGS), (**d**) Lithofacies 4: massive friable fine sandstone (MFFGS) and (**e**) Lithofacies 5: massive very fine grained sandstone (MVFGS)

during burial. These lithofacies reveal no evidence of grain alteration such as feldspar dissolution, quartz growth and cementation as observed for MCGS. It exhibits moderately abundant occurrence of calcite rock fragment (Fig. 6b) and 31% fine-grained fraction composition, suggesting deposition in low-energy subtidal environment of variable hydrodynamics (Abdulrahman et al. 2014). The observed opaque minerals include siderite, iron oxide, clays and calcite, which fill the intergranular pore spaces (Fig. 6d) and

pore throats (Fig. 7). It also comprises moderately abundant and randomly distributed fossil shell fragments (Fig. 6) that are partially filled with fine matrix and serve as intragranular pores (Fig. 7). The grains are predominantly medium grained with random occurrence of coarse grains. The grains are sub-rounded to rounded with high sphericity, suggesting intercalation of loose transgressive sands from coastal to coastal marine deposit (Tan et al. 1999). The grains are moderately compacted, indicating early stage compaction

Fig. 4 Petrography of rock fabric and pore attributes to variations. (**a**) Mineral alteration, (**b**) a XPL of opaque FeO, siderite and clay fractions filling pore spaces, (**c**) Quartz growth/cement and pore attribute modification, (**d**) Feldspar dissolution in MCGS Lithofacies (WB C4B7) sandstone and kaolinite filling a pore (red arrow) at depth 1399.55 m from WB field
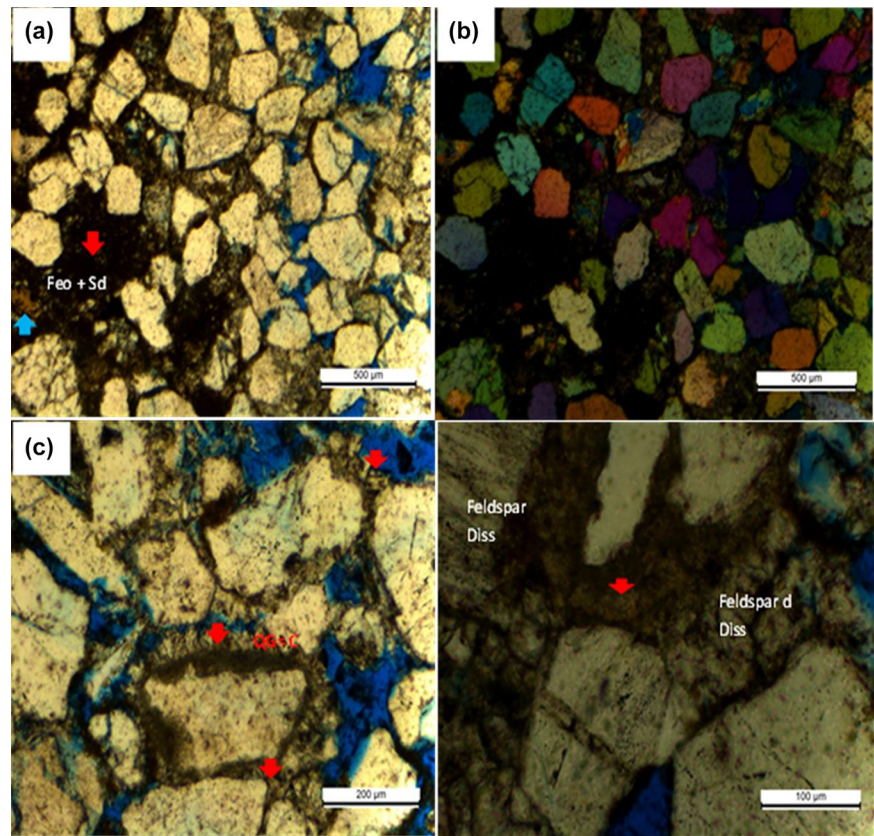
Fig. 5 SEM images of representative photomicrographs of massive coarse-grained sandstone (MCGS) showing different pore types: (**a**) grain shapes, sorting/packing, (**b**) fine-grained matrix fraction obliterating intergranular pores, (**c**) fracture pore and quartz growth reduces pore, (**d**) quartz growth obliterates intergranular pore space and throat in this lithofacies
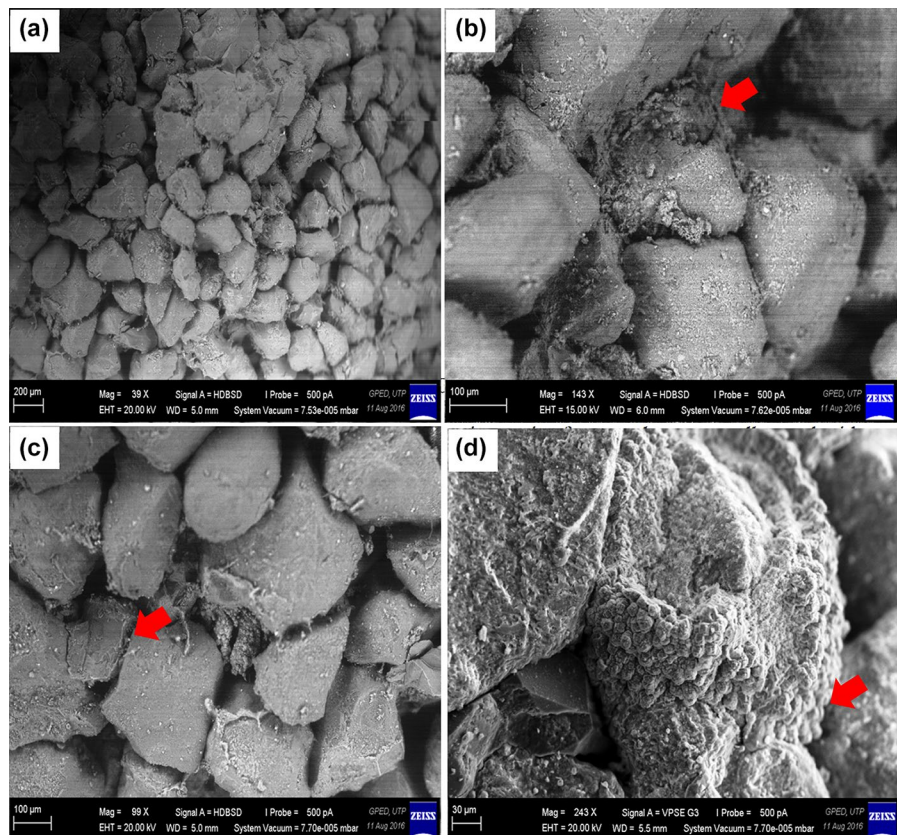
Fig. 6 Petrography of rock fabric variations. (**a**) Embedded fossil shell filled with matrix, (**b**) a XPL of opaque FeO, siderite and clay fractions, (**c**) matrix-filled intra-pore, (**d**) matrix infill of intergranular pore in MMGS (WB C14T9) lithofacies sandstone at depth 1770.78 m
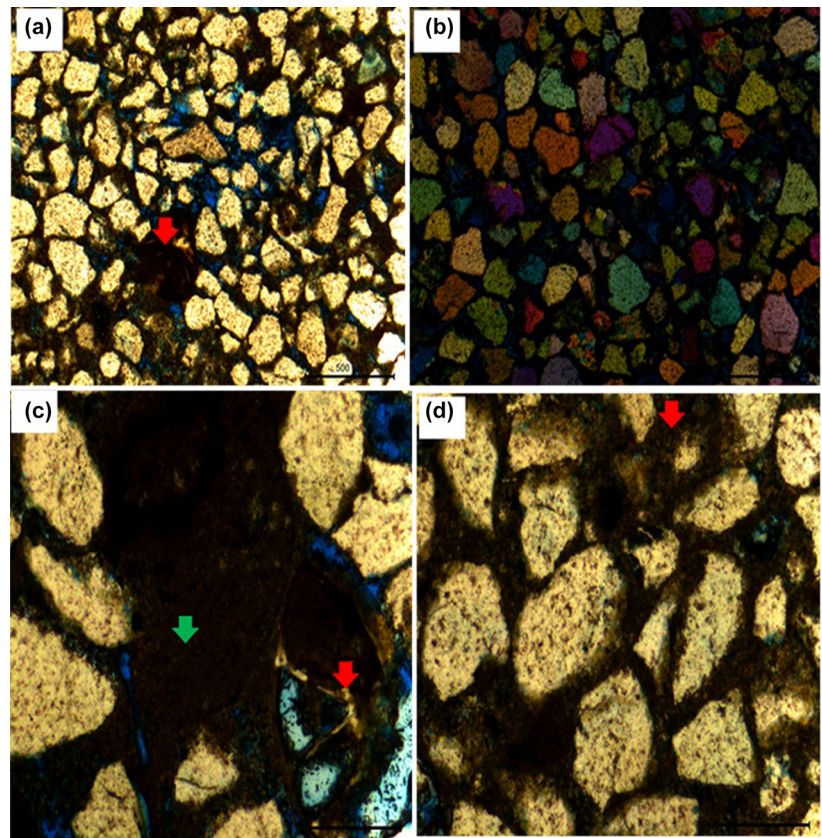
Fig. 7 SEM images of representative photomicrographs of massive medium-grained sandstone (MMGS) showing different pore types: (**a**) grain shapes, sorting/packing, (**b**) fine-grained matrix fraction obliterating intergranular pores, (**c**) fine-grained clogging pore throat and (**d**) fossil shell fragment filled with fine matrix indicated by red arrows
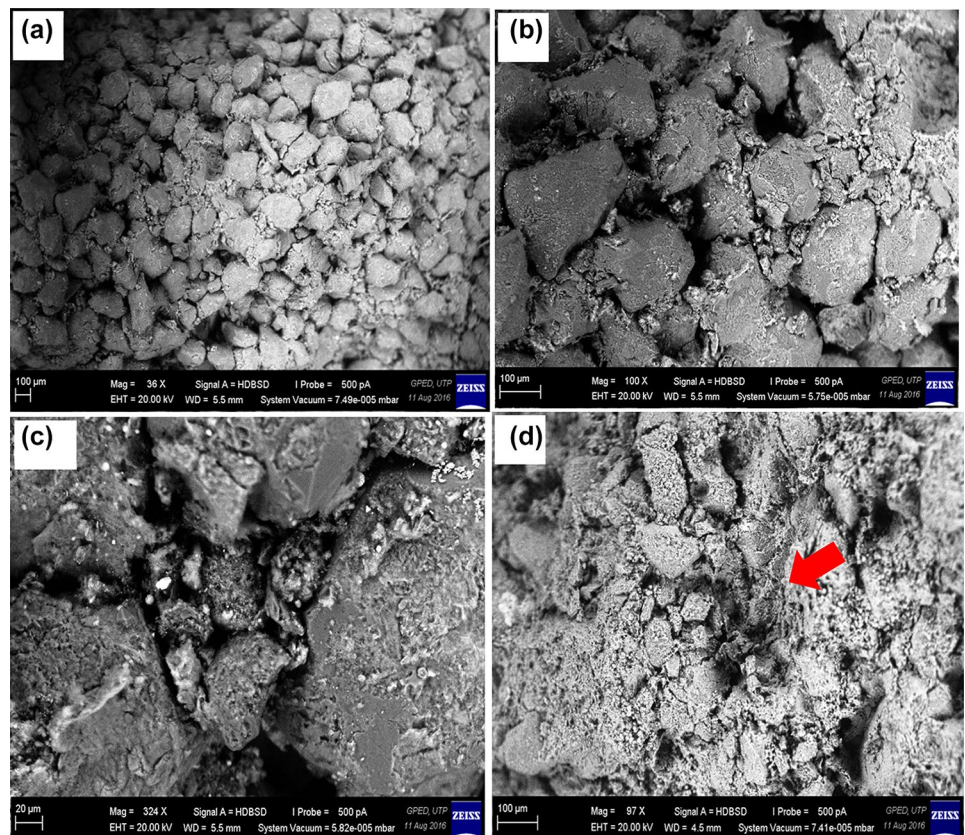
involving readjustment of loose materials in the course of burial (Fig. 6).

The abundance of straight and sutured grain boundaries is also ascribed to early to moderate compaction of sediment during burial. The intergranular porosity of this lithofacies is reduced by pore-filling fine-grained fraction. The average porosity of the lithofacies is 26%.

Lithofacies 3: massive fine-grained sandstone lithofacies (MFGS)

19 representative samples were selected for the massive fine-grained sandstones (MFGS) lithofacies (Fig. 3). Thin-section images obtained under both plane and cross-polarized lights show moderately sorted and medium to fine quartz grains. The quartz grains are mainly monocrystalline, with random and moderate occurrence of medium-sized grains (Fig. 9), which is ascribed to the intrusion of coastal to coastal-fluviomarine sand deposited northwestwards of the prograding delta since the Middle Miocene (from Cycle IV onwards) (Abdulrahman et al. 2014). The lithofacies exhibits minor occurrence of K-feldspar dissolution (Fig. 8), indicating early stage of diagenesis after deposition (Boggs 2009). The quartz grains vary from sub angular to sub-rounded (Fig. 9), due to relatively far distance from source and several cycles of transport and abrasion (Boggs 2009). This

lithofacies is characterized by significant amount of pore-filling fine-grained fractions that obliterate intergranular pores (Fig. 9), which is indicative of low-energy depositional environment and thus interpreted as wave-dominated middle to upper shoreface environment. Porosity distribution in this lithofacies averages at 16% including intrapores (developed within embedded shell fragments; Fig. 9) and matrix-fracture porosity (Fig. 9). The thin sections show moderate abundance of both float and point contacts, which is consistent with the inferred slight to moderate compaction during burial, although random occurrence of concavo-convex contacts is observed in regions with high rock fragments and fine-grained fractions which modified the intergranular pore spaces.

Lithofacies 4: massive friable fine-grained sandstone lithofacies (MFFGS)

23 samples were selected for the massive fine-grained sandstones (MFFGS) (Fig. 1). Petrographic description (Fig. 10) of this lithofacies in plane polarized and cross polar show moderate dissolution of K-feldspar mineral (Fig. 11), dominance of fine-grained quartz, as well as the presence of rock fragments and pore-filling fine siderite (Fig. 11) and rectorite clay fractions (Fig. 11). These pore-filling minerals are a distinctive petrographic feature of this lithofacies. The

Fig. 8 Petrography of rock fabric variations: (**a**) fine-grained quartz mixed with rock fragments, (**b**) a XPL of calcite, FeO and siderite fraction, (**c**) shell fragment-intra-pore, (**d**) an altered K-feldspar grains in MFGS (WB5 C1B5) lithofacies sandstone at depth 1496.42 m
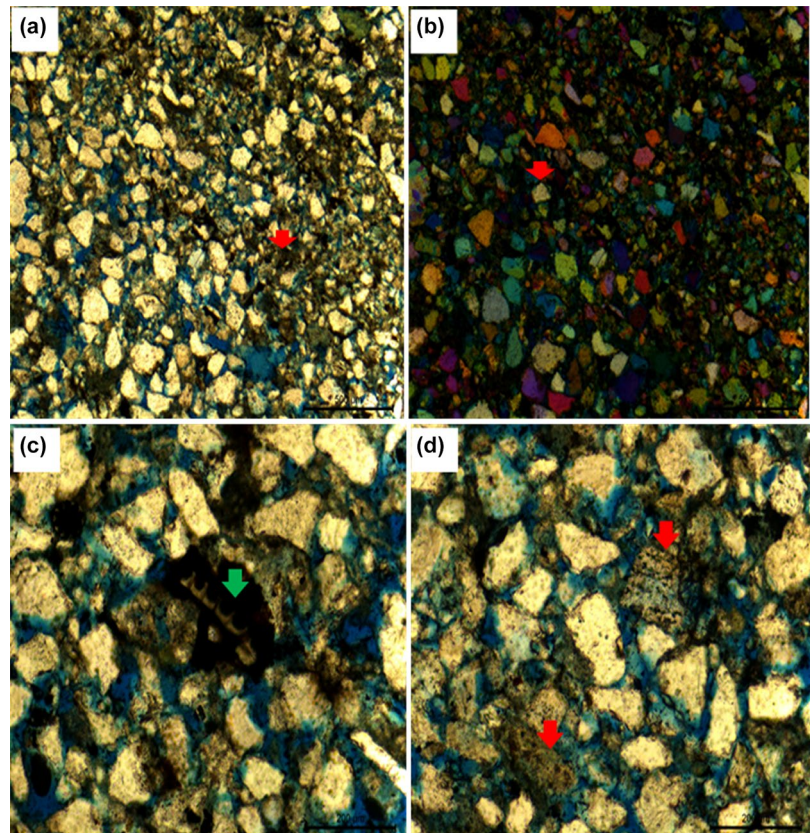
Fig. 9 SEM images of representative photomicrographs of massive fine-grained sandstone (MFGS) showing different pore types: (**a**) grain shapes, sorting/packing, (**b**) fine-grained matrix fraction obliterating intergranular pores, (**c**) matrix-fracture pore and (**d**) matrix-fracture pore indicated by red arrows
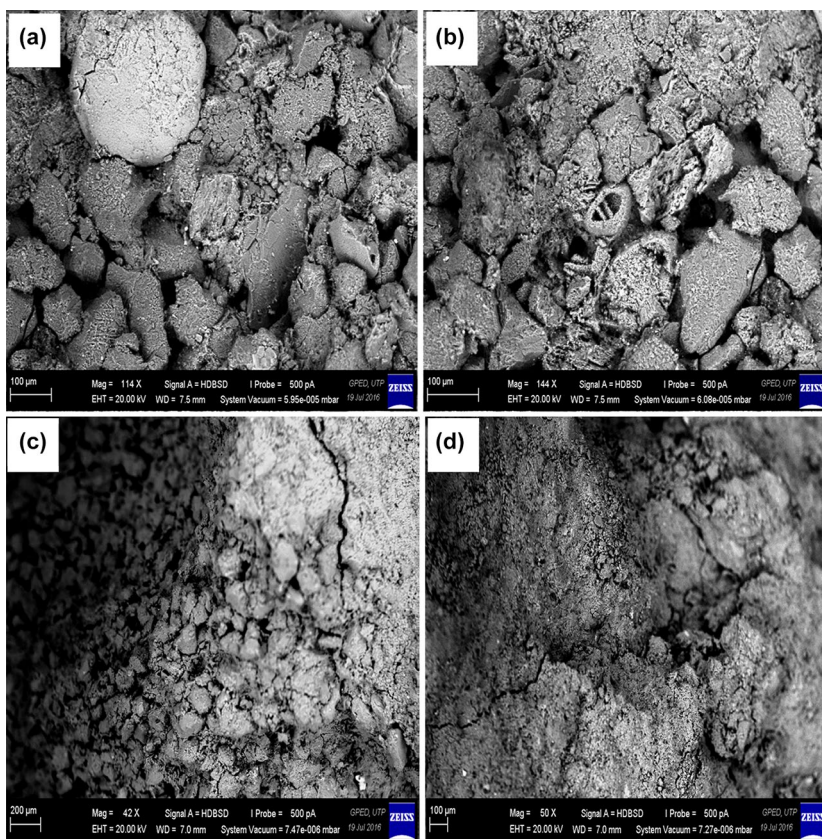
Fig. 10 Petrography of rock fabric variations. (**a**) A lamina boundary of medium-fine grained, (**b**) a XPL of pore-filling iron oxide, rectorite and siderite matrix, (**c**) a wide matrix-fracture pore, (**d**) an extensive matrix-fracture pore in MFFGS (WK`12T4) lithofacies sandstone at depth 1343.8 m
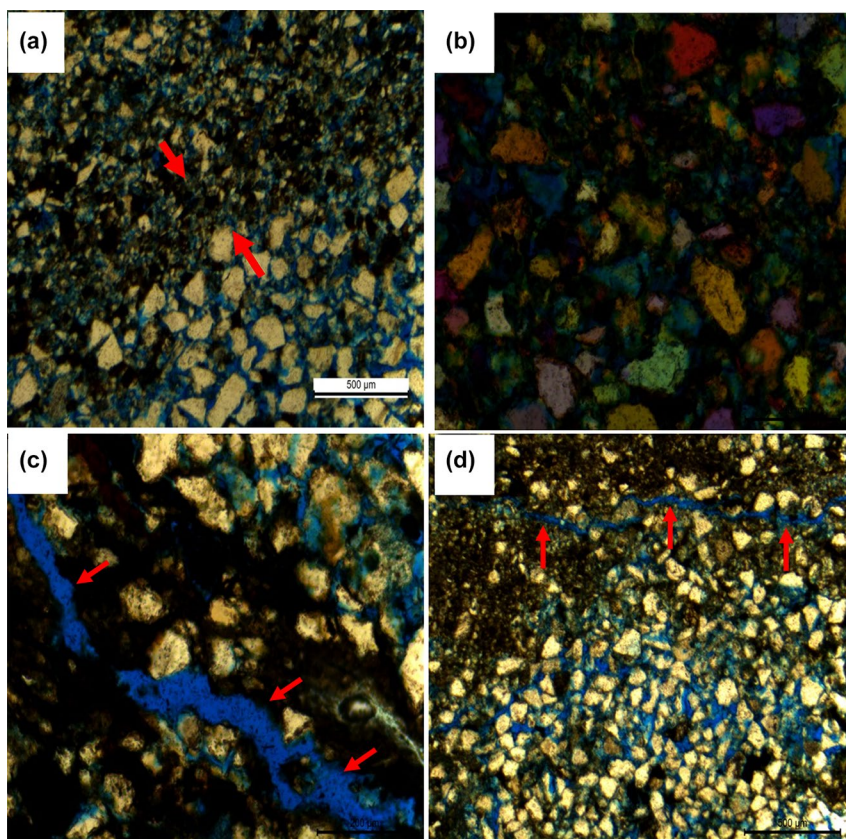
Fig. 11 SEM images of representative photomicrographs of massive friable fine-grained sandstone (MFFGS) showing different pore types: (**a**) grain shapes, sorting/packing, (**b**) rectorite clay mineral occludes intergranular pore space and pore throat, (**c**) red arrows indicate matrix-fracture pore and (**d**) matrix-fracture pore and feldspar dissolution indicated by red and green arrows, respectively
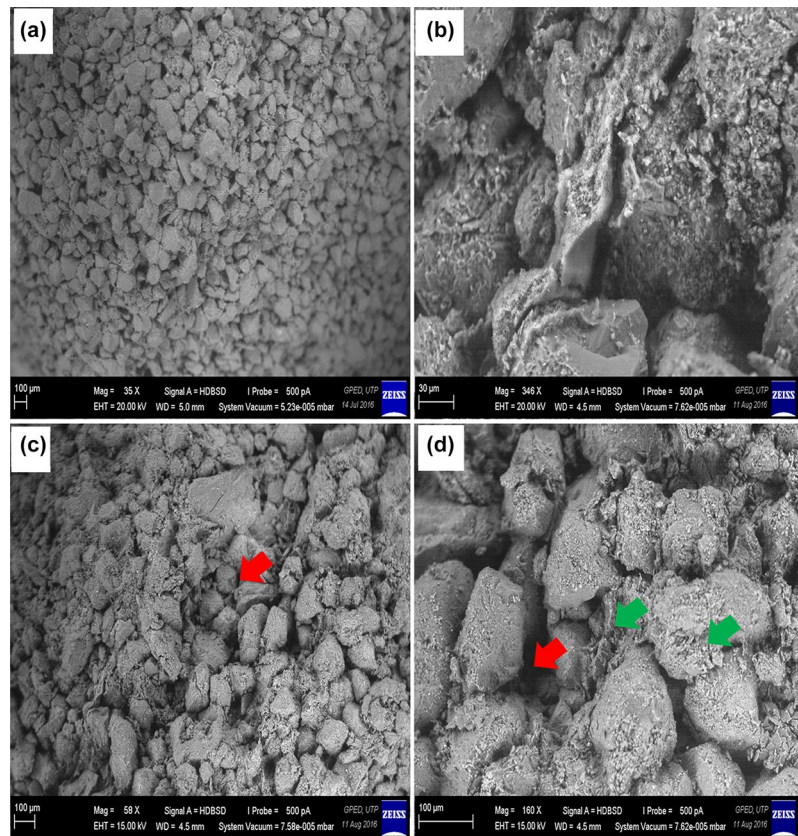
fabric reveals lamina boundary (red arrows) characterized by interbedded monocrystalline medium- to fine-grained silt that forms horizontal laminations (Fig. 10), which are ascribed to cyclic changes in sediments supply in the delta mainly due to variation in depositional energies (Tucker 2003). It exhibits high composition of siderite, iron oxides, clay and carbonate material that occlude intergranular pore spaces (Fig. 10). The monocrystalline quartz and matrix comprise 21% and 48% of the framework, respectively. The framework grains show straight boundary contacts with no suturing (Fig. 10). Long and floating grain contacts are also present within the lithofacies, indicative of intertidal sand flat with variable hydrodynamic activity. The lithofacies exhibit both intergranular and narrowly elongated matrix-fracture porosity types (Fig. 10) with an average porosity of 13%. There exhibit moderate to poorly sorted grains range from angular to subangular in shape (Fig. 11).

Lithofacies 5: massive very fine grained sandstone lithofacies (MVFGS)

19 samples were selected for the massive fine-grained sandstones (MVFGS) lithofacies (Fig. 3). Representative thin sections under plane-polarized and cross-polarized light (Fig. 12) show the presence of larger composition of opaque fine matrix (Fig. 12) compared to other lithofacies.

The framework comprises 26% monocrystalline quartz with minor occurrence of polycrystalline quartz (Fig. 12). The dominant matrix composition of approximately 58% is indicative of deposition in low-energy environment (Boggs 2009). The intergranular pore spaces are infilled with the matrix material (Fig. 12). The abundance of matrix-fracture porosity (Fig. 12) is attributed to increase in pore pressure and temperature with depth (Bjørlykke et al. 1989; Nelson 2001). The framework grains are subangular, sub-rounded to rounded (Fig. 13), and moderate to poorly sorted, indicative of relatively far distance from sediment source, but with low-energy transport (Folk and Ward 1957; Pettijohn et al. 1973). The depositional environment of this lithofacies is interpreted as wave-dominated lower to middle shoreface. Porosity in this lithofacies is mainly matrix-fracture averaged at 22%.

Evaluation of reservoir quality index in relation to Flow Zone Indicator (FZI) in the sandstone lithofacies

The Flow Zone Indicator (FZI) is based on the concept of Reservoir Quality Index (RQI) adopted from an earlier study (Amaefule et al. 1993). The FZI approach involves the clustering of different sandstone lithofacies of similar internal textural grain–pore compositions and petrophysical

Fig. 12 Petrography of rock fabric variations. (**a**) Radial matrix-fracture pore system, (**b**) a crossed polar of opaque dark siderite, iron oxide of pore-filling matrix, (**c**) a granule size quartz grain with matrix-fracture pore, (**d**) a low-magnification matrix-fracture pore in MVFGS (WL4C13T7) lithofacies sandstone at depth at 1466.2 m
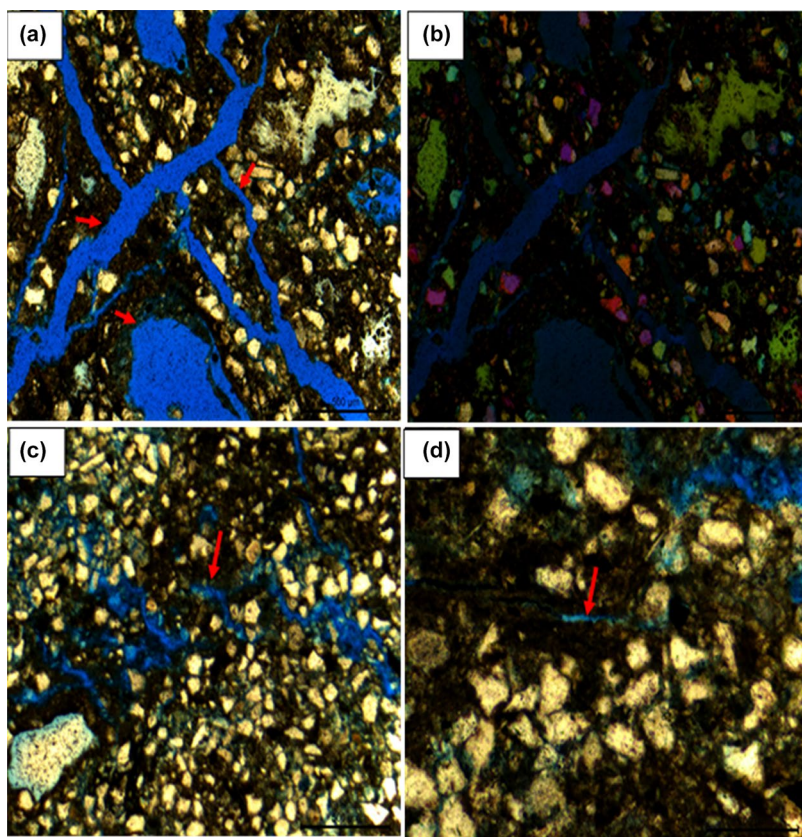
Fig. 13 SEM images of representative photomicrographs of massive very fine grained sandstone (MVFGS) showing different pore types: (**a**) grain shapes, poorly sorted, (**b**) fine-grained and carbonate fragment clogging intergranular pore space and pore throat, (**c**) grains in float and point contact packing pores filled by fine grained matrix, (**d**) fine-grained matrix-fracture pore indicated by red
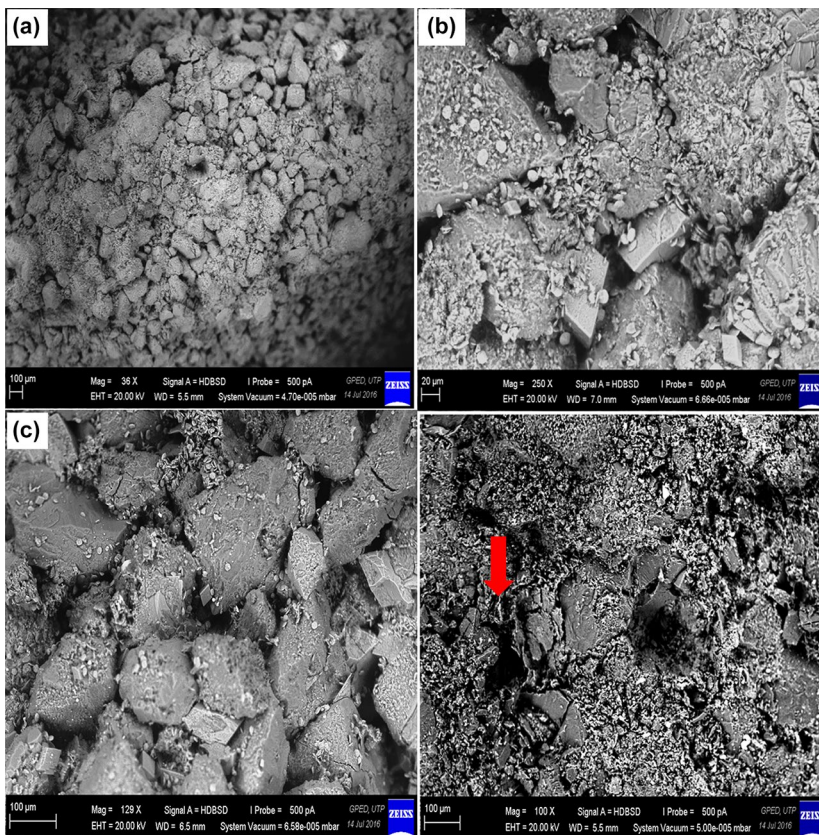
properties (Ebanks Jr 1987). Porosity and permeability data obtained from the Helium porosimetry system were used to determine Flow Zone Indicator (FZI). The plot of RQI against φz based on lithofacies shows a null fluid zone indicator (Amaefule et al. 1993; Tiab and Donaldson 2015). The R^2 value represents the slope of FZI plot for the HFUs. As observed from the plot for the 97 samples (Table 1), lithofacies with similar grain–pore compositions (Fig. 14) and pore attributes are located on the same Flow Zone Indictor (FZI). The plot reveals five main HFUs within the five different sandstone lithofacies varying from 0.01 to 0.08 which are discussed in underlying subsections.

HFU 1

This unit comprises massive very fine grained sandstone (MVFS) and massive medium-grained sandstone lithofacies (MMGS). The FZI value for this HFU is 0.39 with 40% composition from each of the lithofacies. The similarity in fluid characteristics of this unit is attributed to similar percentages of moderately coarse and medium-rounded to well-rounded grains, and high amounts of pore-filling siderite (Figs. 11, 12, 13) and rectorite (Fig. 11), which resulted in a wide variation in porosity range from 17 to 33% with an average of 25% (Table 1). This varied porosity accounts for the deviations in plotted RQI vs. φz values (Fig. 14).

The moderate decrease in FZI value within this unit due the variable fluid flow characteristics has caused high surface area, tortuosity and low Flow Zone Indicator (FZI) value of R^2 of 0.39 (Amaefule et al. 1993; Tiab and Donaldson 2015) within the HFU.

HFU 2

The unit is characterized by four different lithofacies at variable percentages. The total percentage composition of each of four sandstone lithofacies includes massive fine-grained sandstones (MFGS) at 31%, massive very fine grained sandstone (MVFGS) at 15% composition, massive medium-grained sandstone (MMGS) and massive coarse-grained sandstone (MCGS) at 27%, respectively. The plotted RQI vs. φz values for the unit revealed a R^2 of 0.8814 for FZI (Fig. 14). The relatively high R^2 is attributed to varying abundance of coarse- and medium-rounded grains that potentially facilitate low surface area and tortuosity (Amaefule et al. 1993; Tiab and Donaldson 2015) instigated by porosities that vary from 14 to 34%, with an average of 23%. The unit also reveals high permeability that varies from 30.8 to 2980 mD with an average of 665 mD. The improved plot of RQI vs. φz values suggests the sum contribution of grain–pore composition in MFGS (Fig. 13) and MCGS lithofacies with moderate abundance of pore-filling (quartz growth/cement and siderite mineral), as shown in Figs. 4

and 6. The combined effect of grain–pore composition of MFGS and MVFG as shown in Figs. 9, 11 and 13 accounts for the relatively lower fluid flow characteristics in this unit, while the effect of MFGS and MCGS lithofacies improved the FZI value (R^2 of 0.8814) by lowering the surface area and decreases pore tortuosity (Amaefule et al. 1993; Tiab and Donaldson 2015).

HFU 3

This unit is characterized by 43% massive medium-grained sandstone (MMGS) and 29% each of massive friable fine-grained sandstone (MFFGS) and massive coarse-grained sandstone (MCGS) lithofacies (Table 1). The abundance of the grain–pore supportive properties in MMGS improved the FZI value of this unit ($R^2 = 0.8999$) slightly above that of HFU2. The consistency in the fluid characteristics of this unit (Fig. 14) is attributed to their internal grain–pore composition and low pore-reducing mineral that potentially necessitate low surface area and tortuosity (Amaefule et al. 1993; Tiab and Donaldson 2015). The dispersion and random distribution of the values are attributed to the intergranular pore-filling siderite (Fig. 11) present in MFFGS at 29%. Thus, the porosity of the HFU varies from 12 to 32% with an average of 21%. The matrix mineral (siderite) disrupts fluid flow in this unit, which accounts for the wide permeability range of 38.5–2723.8 mD with an average of 889.9 mD. These result in low surface area and tortuosity (Amaefule et al. 1993; Tiab and Donaldson 2015), and moderately high Flow Zone Indicator (FZI) of $R^2 = 0.8999$ in this unit.

HFU 4

This unit comprises different proportions of all five lithofacies (see Table 1). The massive very fine grained sandstone, massive friable fine-grained sandstone (MFFGS), massive fine-grained sandstone (MFGS), massive coarse-grained sandstone (MCGS) and massive medium-grained sandstones (MMGS) make up 16%, 47%, 21%, 5% and 11% of this unit, respectively. The variations in the internal grain–pore framework and intergranular pore-filling siderite matrix composition (Fig. 14) in each of the lithofacies sandstone within this unit result in a wide range of porosity from 9 to 24% with an average of 14%, and permeability range of 30.8–2737 mD with an average of 356 mD.

The abundance of medium to coarse and sub-rounded to rounded grains with high occurrence of matrix-fracture porosity in the massive fine-grained sandstone lithofacies (Fig. 12) accounts for the high permeability values, resulting in the existence of low surface area, tortuosity (Amaefule et al. 1993; Tiab and Donaldson 2015) and moderately higher Fluid Zone Indicator (FZI) value (R^2) of 0.8637 within this unit compared to HFUs 2 and 3.

Table 1 Plotted values for RQI against φz for each of the lithofacies

Sandstone lithofacies	Permeability (mD)	Porosity (%)	φz = φ/(1-φ)	RQI	FZI = RQI/φz
MVFS	38.5	0.27	0.369863	0.007216	0.01951
MVFS	46.2	0.28	0.388889	0.007622	0.019599
MVFS	53.9	0.24	0.315789	0.009605	0.030416
MMGS	58.5	0.22	0.282051	0.01092	0.038716
MMGS	409.6	0.33	0.492537	0.01926	0.039104
MMGS	424.3	0.33	0.492537	0.01959	0.039774
MMGS	409.6	0.32	0.470588	0.01986	0.042203
MFGS	105.2	0.24	0.315789	0.01342	0.042497
MMGS	424.3	0.32	0.470588	0.02021	0.042946
MVFS	61.6	0.21	0.265823	0.01174	0.044165
MFGS	126.2	0.24	0.315789	0.01469	0.046518
MVFS	46.2	0.19	0.234568	0.01123	0.047875
MCGS	2500.2	0.27	0.369863	0.01839	0.049721
MVFS	30.8	0.17	0.204819	0.01025	0.050044
MMGS	365.8	0.29	0.408451	0.02071	0.050704
MVFS	53.9	0.19	0.234568	0.01213	0.051712
MFGS	105.2	0.22	0.282051	0.01464	0.051905
MMGS	219.5	0.25	0.333333	0.01861	0.05583
MMGS	321.9	0.27	0.369863	0.02087	0.056426
MVFS	53.9	0.18	0.219512	0.01281	0.058357
MFGS	120.9	0.21	0.265823	0.01644	0.061846
MMGS	424.3	0.27	0.369863	0.02396	0.064781
MCGS	1184.2	0.33	0.492537	0.03274	0.066472
MMGS	453.5	0.27	0.369863	0.02477	0.066971
MVFS	77	0.18	0.219512	0.01531	0.069746
MCGS	1302.7	0.32	0.470588	0.03542	0.075268
MVFS	30.8	0.14	0.162791	0.01245	0.076479
MVFS	30.8	0.14	0.162791	0.01245	0.076479
MCGS	1184.3	0.31	0.449275	0.03486	0.077592
MFGS	126.2	0.19	0.234568	0.01857	0.079167
MFGS	126.3	0.19	0.234568	0.01857	0.079167
MFGS	105.2	0.18	0.219512	0.01789	0.081499
MFGS	105.2	0.18	0.219512	0.01789	0.081499
MMGS	482.8	0.25	0.333333	0.02759	0.08277
MMGS	482.8	0.25	0.333333	0.02759	0.08277
MFGS	110.4	0.18	0.219512	0.01833	0.083503
MMGS	424.3	0.24	0.315789	0.02695	0.085342
MVFS	53.9	0.15	0.176471	0.01537	0.087097
MFGS	105.2	0.17	0.204819	0.01894	0.092472
MMGS	351.1	0.22	0.282051	0.02674	0.094805
MCGS	2842.3	0.34	0.515152	0.04924	0.095584
MCGS	2908.1	0.34	0.515152	0.0498	0.096671
MCGS	2552.8	0.33	0.492537	0.04808	0.097617
MMGS	468.2	0.23	0.298701	0.02954	0.098895
MCGS	1185.4	0.28	0.388889	0.03861	0.099283
MFGS	52.6	0.14	0.162791	0.01627	0.099944
MMGS	482.8	0.23	0.298701	0.02999	0.100401
MMGS	395.1	0.22	0.282051	0.02837	0.100585
MFFGS	160.8	0.18	0.219512	0.02212	0.100769
MCGS	2552.8	0.32	0.470588	0.04958	0.105358

Table 1 (continued)

Sandstone lithofacies	Permeability (mD)	Porosity (%)	$\phi z = \phi/(1-\phi)$	RQI	$FZI = RQI/\phi z$
MFFGS	142.9	0.17	0.204819	0.02208	0.107802
MCGS	2013.3	0.30	0.428571	0.04696	0.109573
MMGS	190.2	0.18	0.219512	0.02406	0.109607
MCGS	1776.4	0.29	0.408451	0.04564	0.111739
MFFGS	160.8	0.17	0.204819	0.02342	0.114345
MVFS	38.5	0.12	0.136364	0.01624	0.119093
MMGS	292.6	0.19	0.234568	0.02827	0.120519
MFFGS	142.9	0.16	0.190476	0.02346	0.123165
MCGS	2368.5	0.29	0.408451	0.05295	0.129636
MCGS	2190.9	0.28	0.388889	0.05249	0.134974
MFFGS	178.7	0.16	0.190476	0.02623	0.137708
MFGS	99.9	0.14	0.162791	0.02242	0.137723
MCGS	2723.8	0.29	0.408451	0.05651	0.138352
MFFGS	107.2	0.14	0.162791	0.02322	0.142637
MVFS	30.8	0.10	0.111111	0.01743	0.15687
MFFGS	303.8	0.17	0.204819	0.03219	0.157163
MFFGS	435.0	0.18	0.219512	0.03638	0.165731
MMGS	890	0.21	0.265823	0.04461	0.167819
MFFGS	160.8	0.14	0.162791	0.02844	0.174703
MVFS	38.5	0.10	0.111111	0.01948	0.17532
MFGS	220	0.15	0.176471	0.03105	0.17595
MFFGS	170.2	0.14	0.162791	0.02926	0.17974
MFFGS	178.7	0.14	0.162791	0.02998	0.184163
MFGS	94.6	0.12	0.136364	0.02545	0.186633
MFGS	99.9	0.12	0.136364	0.02615	0.191767
MVFS	30.8	0.09	0.098901	0.01936	0.195751
MFFGS	214.4	0.14	0.162791	0.03284	0.201731
MMGS	720	0.18	0.219512	0.04681	0.213246
MCGS	2737.1	0.24	0.315789	0.06845	0.216758
MFFGS	89.4	0.11	0.123596	0.02699	0.218374
MFGS	94.6	0.11	0.123596	0.02776	0.224604
MFFGS	196.6	0.13	0.149425	0.03387	0.226668
MFFGS	71.5	0.10	0.111111	0.02655	0.23895
MFFGS	125.1	0.11	0.123596	0.03193	0.258343
MFFGS	125.1	0.11	0.123596	0.03193	0.258343
MFGS	94.6	0.10	0.111111	0.03054	0.27486
MFFGS	285.9	0.12	0.136364	0.04424	0.324427
MVFS	7.7	0.05	0.052632	0.01743	0.33117
MFFGS	89.4	0.09	0.098901	0.03299	0.333566
MFFGS	89.4	0.09	0.098901	0.03299	0.333566
MFFGS	142.9	0.10	0.111111	0.03754	0.33786
MFGS	21.1	0.05	0.052632	0.02885	0.54815
MFFGS	89.4	0.07	0.075269	0.04241	0.563447
MVFS	23.1	0.05	0.052632	0.03018	0.57342
MFFGS	35.7	0.04	0.041667	0.0469	1.1256
MFGS	21	0.03	0.030928	0.04796	1.550707
MVFS	15.4	0.02	0.020408	0.06161	3.01889
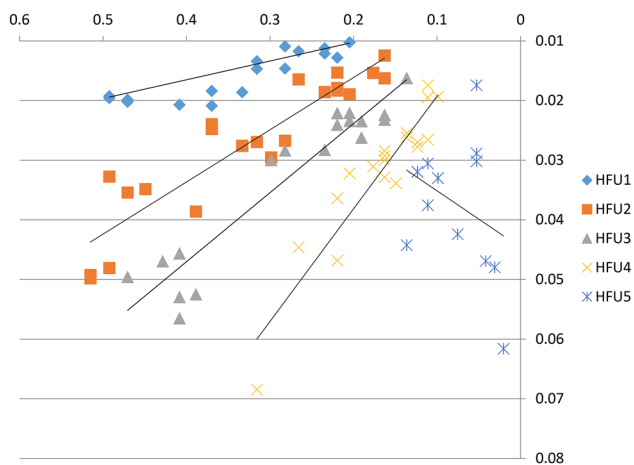
Fig. 14 RQI vs. ɸz indicating five hydraulic fluid units (HFU) in five sandstone lithofacies

HFU 5

This unit comprises 57% massive fine-grained sandstones; (MFFGS), 21% massive fine-grained sandstone (MFGS) and 21% massive very fine grained (MVFG) (see Table 1). The very low Fluid Zone Indicator (FZI) value (R^2) of 0.114 could be attributed to the extremely high intergranular pore-filling siderite matrix that obliterates pore spaces (Figs. 11, 12), leading to a wide porosity range of 2–12% with an average of 7%, and permeability range of 7.7–280.9 mD with an average of 83.9 mD. This wide range of porosity and permeability accounts for the dispersal of plotted FZI values far away from the straight line, resulting in the very low FZI value (R^2) of 0.114, which is indicative of very high surface area and tortuosity (Amaefule et al. 1993; Tiab and Donaldson 2015). The moderately high permeability values of this unit can be attributed to the randomly connected intergranular pore spaces and matrix-fracture present in the unit.

Conclusion

The study defined five lithofacies in the five studied exploratory wells of West Baram Delta Offshore, Sarawak. 5 hydraulic flow units (HFUs) were subsequently identified based on the flow unit characteristics of these reservoir lithofacies using the plot of reservoir quality index (RQI) against normalized porosity (ɸz). The very fine to fine-grained sandstone lithofacies exhibited moderate to high matrix fractions and moderate to poor sorting, suggesting high tortuosity, surface area and hence characterized by low Flow Zone Indicator (FZI). On the other hand, the medium to coarse-grained lithofacies exhibited very low to low matrix fractions, medium to coarse grain sizes and moderate to well sorting, signifying lower tortuosity, surface area and hence

characterized by relatively higher Flow Zone Indicator (FZI). Therefore, a hydraulic flow unit (HFU) can be formed by more than one sandstone lithofacies that exhibit similar fluid characteristic attributes, regardless of the difference in depositional environment and diagenetic processes undergone. The HFU scattered plot can thus serve as qualitative model for the characterization of flow unit characteristics in a well-comprising different lithofacies, particularly for field development plans in the West Baram Delta.

References

Abdullah R (2012) Oil & gas industry–opportunities and challenges ahead, An Halliburton Power Point Presentation. Presented on 30th May 2012

Abdulrahman AH, Menier D, Mansor YM (2014) Sequence stratigraphy modeling and reservoir Architecture of the shallow marine succession of Baram Field, West Baram Delta offshore Sarawak, East Malaysia. Mar Petrol Geol 4:687–703

Amaefule JO, Altunbay M, Tiab D, Kersey DG, Keelan DK (1993) Enhanced reservoir description: using core and log data to identify hydraulic (flow) units and predict permeability in uncored intervals/wells. In: Paper presented at the SPE annual technical conference and exhibition

Archie GE (1952) Classification of carbonate reservoir rocks and petrophysical considerations. AAPG Bull 36(2):278–298

Bjørlykke K, Ramm M, Saigal GC (1989) Sandstone diagenesis and porosity modification during basin evolution. Geol Rundsch 78(1):243–268

Boggs S (2009) Petrology of sedimentary rocks. Cambridge University Press, Cambridge

Cullen A (2014) Reprint of: nature and significance of the West Baram and Tinjar Lines, NW Borneo. Mar Pet Geol 58:674–686

Davies D, Vessell R (1996) Identification and distribution of hydraulic flow units in a heterogeneous carbonate reservoir: North Robertson Unit, west Texas. In: Paper presented at the Permian Basin Oil and Gas Recovery Conference

Doust H (1981) Geology and exploration history of offshore central Sarawak. 117–132

Ebanks Jr W (1987) Flow unit concept-integrated approach to reservoir description for engineering projects. AAPG (Am. Assoc. Pet. Geol.) Bull.;(United States), 71(CONF-870606-)

Folk RL, Ward WC (1957) Brazos River bar [Texas]; a study in the significance of grain size parameters. J Sed Res 27(1):6–10

Fui HK (1978) Stratigraphic framework for oil exploration in Sarawak. Geol Soc Malays Bull 10:1–14

Hearn C, Ebanks Jr W, Tye R, Ranganathan V (1984) Geological factors influencing reservoir performance of the Hartzog Draw Field, Wyoming. J Pet Technol 36(08):1,335–331,344

Johnson H, Kuud T, Dundang A (1989) Sedimentology and reservoir geology of the Betty field, Baram Delta Province, offshore Sarawak, NW Borneo. Bull Geol Soc Malays 25:119–161

Khatib H (2012) IEA world energy outlook 2011—a comment. Energy Policy 48:737–743

Korvin G (2016) Permeability from microscopy: review of a dream. Arab J Sci Eng 41(6):2045–2065

Lambiase JJ, bin Abdul Rahim AA, Peng CY (2002) Facies distribution and sedimentary processes on the modern Baram Delta: implications for the reservoir sandstones of NW Borneo. Mar Pet Geol 19(1):69–78

Latief AI, Ridzuan AI, Faehrmann PA, Macdonald AC, Arina W, Rahman G (2012) An innovative static modeling approach to handle a complex giant within a compressed timeframe; a Case Study of Baram Oil Field, Offshore Sarawak, East Malaysia. In: Paper presented at the SPE Asia Pacific Oil and Gas Conference and Exhibition

Madon M (1999) Geological setting of Sarawak. The petroleum geology and resources of Malaysia, Kuala Lumpur, 273–290

Madon M, Kim CL, Wong R (2013) The structure and stratigraphy of deepwater Sarawak, Malaysia: implications for tectonic evolution. J Asian Earth Sci 76:312–333

Nelson R (2001) Geologic analysis of naturally fractured reservoirs. Gulf Professional Publishing, Houston

Nooruddin HA, Hossain ME (2011) Modified Kozeny–Carmen correlation for enhanced hydraulic flow unit characterization. J Pet Sci Eng 80(1):107–115

Onuh HM, David OO, Onuh CY (2017) Modified reservoir quality indicator methodology for improved hydraulic flow unit characterization using the normalized pore throat methodology (Niger Delta field as case study). J Pet Explor Prod Technol 7(2):409–416

Pauzi N, Low F, Abas A, Juwaini A, Maksari H (1999) Revitalizing The West Lutong Field. In: Paper presented at the SPE Asia Pacific Improved Oil Recovery Conference

Pettijohn F, Potter P, Siever R (1973) Sand and sandstone. New York/Heidelberg/Berlin, pp 618

Powers MC (1953) A new roundness scale for sedimentary particles. J Sed Res 23(2):117–119

Prince CM, Ehrlich R, Carr MB (1999) The effect of sandstone microfabric upon relative permeability end points. J Petrol Sci Eng 24(2):169–178

Raith MM, Raase PR, Reinhardt JR (2011) Guide to thin section microscopy. University of Bonn, Bonn

Rijks E (1981) Baram Delta geology and hydrocarbon occurrence. Geol Soc Malays Bull 14:1–8

Shenawi SH, White JP, Elrafie EA, El-Kilany KA (2007) Permeability and water saturation distribution by lithologic facies and hydraulic units: a reservoir simulation case study. In: Paper presented at the SPE Middle East Oil and Gas Show and Conference

Tan D, Rahman A, Anuar A, Bait B, Tho CK (1999) West Baram Delta. The Petroleum Geology and Resources of Malaysia, Petroliam Nasional Berhad (PETRONAS), Kuala Lumpur, pp 291–341

Terry RE, Rogers JB, Craft BC (2013) Applied petroleum reservoir engineering. Pearson Education, London

Tiab D, Donaldson EC (2015) Petrophysics: theory and practice of measuring reservoir rock and fluid transport properties: Gulf professional publishing

Tucker ME (2003) Sedimentary rocks in the field. Wiley, Hoboken

Wentworth CK (1922) A scale of grade and class terms for clastic sediments. J Geol 30(5):377–392

Worden R, Morad S (2000) Quartz cementation in oil field sandstones: a review of the key controversies. Quartz cementation in sandstones. Int Assoc Sedimentol Spec Publ 29:1–20

Zhou W, Liang S, Ma D, Tang Z (2014) Statistical verification of hydraulic units in a heterogeneous reservoir of the Liaohe Oilfield. J Earth Sci 25(6):991–1002